



Tuning the interfacial sites between copper and metal oxides (Zn, Zr, In) for CO₂ hydrogenation to methanol



Kristian Stangeland^a, Hans Herrera Navarro^a, Huong Lan Huynh^a, Wakshum Mekonnen Tucho^b, Zhixin Yu^{a,*}

^a Department of Energy and Petroleum Engineering, University of Stavanger, 4036 Stavanger, Norway

^b Department of Mechanical and Structural Engineering and Materials Science, University of Stavanger, 4036 Stavanger, Norway

HIGHLIGHTS

- Catalytic performance is highly sensitive to the Cu-oxide interaction.
- Activity related to the Cu-oxide interfacial sites rather than the Cu surface area.
- ZrO₂ impregnation of Cu/ZnO enhances activity and methanol selectivity.
- Methanol space-time yield of 15.6 mmol·g_{cat}⁻¹·h⁻¹ is achieved for ZrO₂/Cu-ZnO.
- In-Zr mixed oxide sites boosts space-time yield at 270 °C for Cu/ZrO₂/In₂O₃.

ARTICLE INFO

Article history:

Received 29 September 2020

Received in revised form 7 February 2021

Accepted 17 March 2021

Available online 24 March 2021

Keywords:

CO₂ hydrogenation

Methanol

Copper

Indium oxide

Zinc oxide

Zirconium oxide

ABSTRACT

The influence of different metal oxides (ZnO, ZrO₂, In₂O₃) in CO₂ hydrogenation to methanol over Cu-based catalysts was studied. The catalysts were characterized using x-ray diffraction (XRD), thermal gravimetric analysis (TGA), transmission electron microscopy (TEM), N₂-physisorption, N₂O chemisorption, H₂ temperature-programmed reduction (H₂-TPR), and CO₂ temperature-programmed desorption (CO₂-TPD). It was found that impregnating ZrO₂ onto Cu/ZnO enhances the methanol formation rate from 14.7 mmol·g_{cat}⁻¹·h⁻¹ to 15.6 mmol·g_{cat}⁻¹·h⁻¹ (230 °C, 30 bar, 38 000 cm³/(g_{cat} h)), which is attributed to the formation of Cu-ZrO₂ sites. The results also indicate that In-doping of the Cu-based catalysts generates Cu_xIn_y alloys, which seems to inhibit the active sites on the Cu surface. However, new sites for methanol synthesis are present when Cu/ZrO₂/In₂O₃ is prepared by co-precipitation. This is attributed to In-Zr mixed oxide species that increases the methanol formation rate from 53.2 mmol·g_{cat}⁻¹·h⁻¹ to 60.5 mmol·g_{cat}⁻¹·h⁻¹ (270 °C, 30 bar, 140 000 cm³/(g_{cat} h)).

© 2021 The Authors. Published by Elsevier Ltd. This is an open access article under the CC BY license (<http://creativecommons.org/licenses/by/4.0/>).

1. Introduction

Recently, the need to combat the effects of greenhouse gas emissions has generated significant interest in developing various technologies for capturing and transforming CO₂ into useful products. CO₂ hydrogenation to methanol is among the most promising approaches for sustainable production of fuels and chemicals from renewable sources (Aresta et al., 2016). Methanol is currently widely employed within the petrochemical industry to produce various compounds, such as olefins, aromatics, and gasoline. Furthermore, methanol is also increasingly used in fuel blends or as

an alternative fuel in the transportation sector. Methanol synthesis from synthesis gas (CO, CO₂, H₂) is already a well-established industry, which could assist in the development and large-scale implementation of the CO₂-to-methanol process. Provided a sustainable source of hydrogen becomes available at reasonable costs, recycling CO₂ could become economically viable with sufficient political incentives.

The different behavior of metal oxide-promoted Cu-based catalysts, in terms of activity and stability under different feeds, highlights that optimizing the surface-interface structures is a viable strategy for obtaining efficient CO₂-to-methanol catalysts. (Denise and Sneed, 1986; Jansen et al., 2002; Studt et al., 2015; Topsøe et al., 1997; Topsøe and Topsøe, 1999). There is compelling evidence that the strong metal-support interaction (SMSI) due to the partial reducibility of metal oxides plays a key role in

* Corresponding author at: Universitetet i Stavanger, Postboks 8600 Forus, 4036 Stavanger, Norway.

E-mail address: Zhixin.yu@uis.no (Z. Yu).

the CO₂ hydrogenation to methanol over Cu-based catalysts. The Cu/ZnO/Al₂O₃-based catalysts have been utilized for decades in the industrial methanol synthesis process from syngas (CO, CO₂, H₂), which is operated at 200–300 °C and 50–100 bar. Isotopic labeling experiments and DFT calculations indicate that methanol is mainly produced from CO₂ over Cu/ZnO-based catalysts even from syngas under typical reaction conditions (Gaikwad et al., 2020). The promotional effect of ZnO has been attributed to the presence of Zn or ZnO_x species on the Cu surface (Behrens et al., 2012; Fujitani et al., 1997a; Fujitani et al., 1997b; Kattel et al., 2017; Martinez-Suarez et al., 2015; Nakamura et al., 1996), which stabilizes the oxygen-bound intermediates and enhances the methanol synthesis activity. Recent high-pressure operando studies indicate the preformation of a CuZn alloy during reduction and subsequent formation of an active Zn formate intermediate, which is subsequently hydrogenated to methanol (Zabitskiy et al., 2020). This is also supported by computational modeling using DFT and kinetic simulations (Behrens et al., 2012; Kattel et al., 2017; Reichenbach et al., 2018; Zheng et al., 2020).

The Cu-ZrO₂ interfacial sites are widely reported to enhance the activation and transformation of CO₂ into methanol over Cu/ZrO₂-based catalysts (Arena et al., 2008; Fujiwara et al., 2019; Gao et al., 2012; Larmier et al., 2017; Tada et al., 2018a; Tada et al., 2018b). Cu/ZrO₂ catalysts containing different polymeric phases of ZrO₂ have been reported for methanol synthesis, such as monoclinic (*m*-), tetragonal (*t*-), and amorphous (*a*-) ZrO₂ (Jung and Bell, 2002; Rhodes and Bell, 2005; Baiker et al., 1993; Köppel et al., 1998; Ma et al., 2005; Samson et al., 2014; Witton et al., 2016; Tada et al., 2018a). The performance of Cu/ZrO₂-based catalysts is influenced by the metal properties (Cu particle size and dispersion), state of ZrO₂ support (crystalline form and particle size), surface properties (acid, basic and oxygen vacancy concentration), and the metal-support interaction (Li and Chen, 2019). Recently, extensive studies on inverse oxide/Cu systems for CO₂ hydrogenation to methanol has been performed, which indicate superior performance compared to the conventional catalytic structure (Graciani et al., 2014; Senanayake et al., 2016; Chen et al., 2019; Wang et al., 2019b). Lam et al. (Lam et al., 2018) found that Cu domains supported on high surface area silica containing highly dispersed isolated ZrO_x motifs exhibits similar performance as that of Cu/ZrO₂. Wu et al. (Wu et al., 2020) observed that the inverse ZrO₂/Cu catalyst composed of small ZrO₂ islands covering the metallic Cu surface exhibited about 3 times higher mass-specific methanol formation rate compared to the conventional Cu/ZrO₂ catalyst. Recent studies indicate that the direct hydrogenation of CO₂ via the formate intermediate is the dominant reaction pathway over Cu/ZrO₂ catalysts during CO₂ hydrogenation to methanol (Larmier et al., 2017; Wang et al., 2019b; Wu et al., 2020; Ma et al., 2020). However, both CO₂ and CO can be converted to methanol over Cu/ZrO₂ at high rates and the preferred route might be sensitive to the nanostructure of the catalyst and the reaction conditions (Kattel et al., 2016).

Although highly active In₂O₃-based catalysts have been demonstrated (Chou and Lobo, 2019; Frei et al., 2019; Men et al., 2019), the reported activity of In-doped Cu-based catalysts are ambiguous. Słoczyński et al. (Słoczyński et al., 2006) and Sadeghinia et al. (Sadeghinia et al., 2020) found that incorporating a small amount of In into Cu/ZnO-based catalysts significantly reduced the catalytic activity. On the other hand, Shi et al. (Shi et al., 2019) reported synergistic effects between Cu_xIn_y and In₂O₃, resulting in highly selective methanol synthesis catalysts. Gao et al. (Gao et al., 2020) proposed that hydrogen is activated on Cu_x-In_y sites, while the In₂O₃-ZrO₂ phase facilitates CO₂ adsorption and conversion to methanol. Zhang et al. (Zhang et al., 2020) observed that low amounts of In enhanced the methanol formation rate and selectivity of Cu/ZrO₂. The greater reducibility of In₂O₃ compared

to ZnO, ZrO₂, and CeO₂ means that In₂O₃ species migrate readily during reduction and form surface and bulk Cu_xIn_y alloys. However, these studies indicate that ZrO₂ might have a stabilizing effect on In₂O₃ and generate additional In-Zr mixed oxide sites for methanol synthesis.

Elucidating the relationship between the catalytic structure and interfacial sites of Cu-based catalysts can offer valuable insight for developing high-performance CO₂-to-methanol catalysts. Herein, we provide insight into the highly structure-sensitive nature of Cu-based catalysts and the interplay between different metal oxide promoters. It is demonstrated that impregnating Cu/ZnO with ZrO₂ enhances the methanol synthesis activity, which is attributed to the formation of Cu-ZrO₂ interfacial sites for CO₂ activation and conversion to methanol. In contrast, ZnO-doping of Cu/ZrO₂ seems to inhibit the Cu-ZrO₂ interfacial sites. It is also shown that In-doping of Cu/ZrO₂ can enhance the catalyst's performance, whereas the activity is significantly reduced when In is impregnated onto Cu/ZnO. This is linked to a stabilizing effect of ZrO₂ on In₂O₃, resulting in In-Zr mixed oxide sites for CO₂ conversion to methanol. On the other hand, the In₂O₃ species on Cu/ZnO are easily reduced, leading to In migration to the Cu surface, which blocks the active sites. It is also demonstrated that the activity is correlated to the Cu-oxide interaction rather than the Cu surface area.

2. Materials and methods

2.1. Catalyst preparation

The co-precipitated catalysts were prepared following a procedure explained in detail elsewhere (Behrens and Schlögl, 2013). Briefly, an aqueous nitrate solution containing an appropriate ratio of metal nitrates was co-precipitated at a constant pH of 6.5 using sodium carbonate as precipitating agent. The precipitate was aged in the mother liquor for 14 h under vigorous stirring at 65 °C in a sealed cell under a constant flow of N₂. The precipitate was filtered and washed several times with deionized water. The precursors were dried overnight at 90 °C prior to calcination at 350 or 500 °C for 3 h. The co-precipitated catalysts are denoted as CuM-X, where M is ZnO, ZrO₂, or In₂O₃ and X refers to the calcination temperature. The calcined CuZn-350 was impregnated with an In nitrate or Zr nitrate solution to yield a metal content of 1 mol%. Similarly, the calcined CuZr-350 catalyst was impregnated with In nitrate or Zn nitrate. The impregnated samples were dried and calcined again at 350 °C for 3 h. The impregnated samples are denoted as M/CuZn-350 or M/CuZr-350, where M is ZnO, ZrO₂, or In₂O₃. The nominal and real metal content determined from ICP-AES of the prepared catalysts are summarized in Table 1.

2.2. Characterization of catalysts

N₂ adsorption-desorption measurements were obtained at 77 K using a Micromeritics TriStar II instrument. The samples were degassed prior to analysis at 120 °C for 14 h with a Micromeritics VacPrep 061 degas system. The specific surface areas and pore size distribution were determined by the Brunauer-Emmet-Teller (BET) and Barret-Joyner-Halenda (BJH) methods, respectively.

The elemental composition of the catalysts was analyzed by ICP-AES on an Agilent 725-ES apparatus. Typically, 200 mg of sample was dissolved in a boiling HNO₃:HCl mixture with a ratio of 1:3 until complete dissolution of the catalyst. The sample was further diluted and filtered prior to elemental analysis.

The X-ray diffraction (XRD) patterns were recorded on a Bruker-AXS Microdiffractometer (D8 ADVANCE) instrument using a Cu K α radiation source ($\lambda = 1.5406$, 40 kV, and 40 mA). The reduced sam-

Table 1
Nominal and actual metal content of the Cu-based catalysts determined by ICP-AES.

Catalyst	Nominal metal content (mol%)				Metal content determined by ICP-AES (mol%)			
	Cu	Zn	Zr	In	Cu	Zn	Zr	In
CuZn-350	83.3	16.7	–	–	83.2	16.8	–	–
In/CuZn-350	82.5	16.5	–	1.0	82.2	16.5	–	1.3
Zr/CuZn-350	82.5	16.5	1.0	–	82.2	16.7	1.1	–
CuZr-350	83.3	–	16.7	–	89.1	–	10.9	–
CuZrIn-350	82.9	–	16.6	0.5	88.7	–	11.0	0.3
In/CuZr-350	82.5	–	16.5	1.0	88.0	–	10.9	1.1
Zn/CuZr-350	82.5	1.0	16.5	–	87.8	1.0	11.2	–
CuIn-350	83.3	–	–	16.7	84.1	–	–	15.9

ples were passivated in 1% O₂/N₂ before being transferred to the sample holder. The patterns were collected at 2θ of 10–90° with a step interval of 2°/min. The peaks were identified using the Joint Committee on Powder Diffraction Standards (JCPDS) database.

The simultaneous thermal gravimetric (TG) and differential scanning calorimetry (DSC) curves were recorded on Netzsch STA449 Jupiter F3 instrument. In a typical experiment, a small amount of sample (10 mg) was heated from room temperature to 700 °C at a heating rate of 10 °C/min in synthetic air at a flow rate of 20 mL/min.

The morphology of the reduced catalysts was investigated by transmission electron microscopy (TEM) with a JEOL JEM-2100F instrument operated at 200 kV. The reduced-passivated powders were dispersed in ethanol by ultrasonication and deposited on a holey carbon-coated copper grid.

Temperature programmed reduction (H₂-TPR) measurements were conducted using a Micromeritics Autochem II ASAP 2920 instrument. First, the sample was heated to 200 °C in He flow for 30 min. Then, the profiles were recorded by passing a 7% H₂/Ar mixture at 50 mL/min over the sample while the temperature was ramped from ambient to 550 °C at 10 °C/min.

Temperature programmed desorption (CO₂-TPD) was carried out using the same instrument as for H₂-TPR. About 100 mg of sample was pretreated at 200 °C for 30 min under He, reduced at 350 °C for 2 h, and then purged with He for 1 h. CO₂ adsorption was performed with a 6 vol% CO₂/Ar mixture at 50 °C for 1 h. Physically adsorbed CO₂ was removed by purging the sample in He flow for 1 h. CO₂-TPD was carried out under constant He flow (40 mL/min) from ambient to 800 °C at a heating rate of 10 °C/min.

The exposed Cu surface area (SA_{Cu}) was determined by a dissociative N₂O adsorption method using a Micromeritics Autochem 2920 instrument. Before N₂O adsorption, the sample was heated to 200 °C in He flow for 30 min and reduced at 350 °C in 7% H₂/Ar mixture (50 mL/min) for 2 h. Then, He was passed over the sample until the temperature reached 50 °C. The N₂O adsorptive decomposition was carried out in a 1% N₂O/He mixture at 50 °C for 1 h following a procedure described by Van Der Grift et al. (Gervasini and Bennici, 2005; Liang et al., 2019; Van Der Grift et al., 1991). After that, the sample tube was purged with He for 1 h to remove the unreacted N₂O. Finally, the H₂ consumption was determined by a second H₂-TPR experiment from 50 to 400 °C at a rate of 10 °C/min in a 7% H₂/Ar mixture. The Cu surface area (SA_{Cu}) was calculated using Eq. (1).

$$SA_{Cu}(m^2 \cdot g_{cat}^{-1}) = \frac{Y \times SF \times N_A}{C_M \times W_{cat}} \quad (1)$$

where Y is the moles of H₂ consumed in the TPR following N₂O chemisorption, SF is the stoichiometric factor (2), N_A is Avogadro's number (6.022 × 10²³ mol⁻¹), C_M is the number of surface Cu atoms per unit surface area (1.47 × 10¹⁹ atoms·m⁻²), and W_{cat} is the amount of catalyst (g).

2.3. Catalytic activity tests

The CO₂ hydrogenation experiments were carried out in a custom-built fixed-bed continuous-flow reactor. Typically, 0.1 g of the sieved catalyst was mixed with SiC (1 g) and placed in a stainless tube reactor with an internal diameter of 0.5 cm and a length of 50 cm. The catalysts were reduced for 2 h at 350 °C with a heating rate of 2 °C/min by 10% H₂/N₂ (50 mL/min). The reactor was cooled to ambient temperature, pressurized with the reactant gases (H₂/CO₂/N₂ = 3/1/1), and then heated to the desired reaction temperature before the activity tests. Product condensation was avoided by heating the post-reactor lines and valves to 140 °C. On-line analysis of the exit stream was performed with an Agilent 7890B system containing two channels equipped with TCD detectors. A HayeS Q (length 0.25 m, diameter 1 mm, thickness 80/100 μm) and a Mols 5A (length 1.5 m, diameter 1 mm, thickness 80/100 μm) column is used for the separation of H₂, N₂, and CO using He as carrier gas. The CO₂, C₁-C₃ hydrocarbons, and C₁-C₃ oxygenates in the product is separated by a GS-carbonplot column (length 60 m, diameter 0.32, thickness 1.5 μm) using Ar as carrier gas. The CO₂ conversion was calculated utilizing N₂ as internal standard based on Eq. (2). The methanol selectivity (S_{methanol}) and space-time yield of methanol (STY_{methanol}) were calculated using Eq. (3) and Eq. (4), respectively.

$$X_{CO_2}(\%) = \left[1 - \frac{\text{molesCO}_{2,\text{out}}}{\text{molesCO}_{2,\text{in}}} \times \frac{\text{molesN}_{2,\text{in}}}{\text{molesN}_{2,\text{out}}} \right] \times 100 \quad (2)$$

$$S_{\text{methanol}}(\%) = \frac{\text{molesmethanol}_{\text{out}}}{\text{molesmethanol}_{\text{out}} + \text{molesCO}_{\text{out}}} \times 100 \quad (3)$$

$$STY_{\text{methanol}} \left(\text{mmol}_{\text{methanol}} \cdot g_{\text{cat}}^{-1} \cdot h^{-1} \right) = \frac{F_{CO_2,\text{in}} \times X_{CO_2}/100 \times S_{\text{methanol}}/100}{W_{\text{cat}}} \quad (4)$$

where F_{CO₂,in} (mmol/h) is the molar flow rate of CO₂ at the inlet of the reactor and W_{cat} (g) is the amount of catalyst.

3. Results and discussion

3.1. Catalyst characterization

3.1.1. N₂ physisorption

The N₂ physisorption results of the CuZn and CuZr catalysts are summarized in Table 2. The N₂-adsorption-desorption isotherms are shown in the Supporting Information, Figure S1. The BET surface area of the CuZn-350, CuZr-350, and CuZrIn-350 catalysts prepared by co-precipitation are similar in the range of 72–77 m²/g. Furthermore, the pore volume is also comparable for these catalysts (0.17–0.19 cm³/g). The impregnated catalysts exhibit lower BET surface area and pore volume, which might be related to pore blocking or structural changes during the second calcination treatment. The decrease in BET surface area is more significant for In/

Table 2
Structural properties of the CuZn-based and CuZr-based catalysts.

Catalyst	S_{BET} (m^2/g)	Pore volume (cm^3/g)	Pore diameter (nm)	$d_{\text{CuO}(111)}$ (nm)	$d_{\text{Cu}(111)}$ (nm)	$d_{\text{ZnO}(101)}$ (nm)
CuZn-350	72	0.17	7.7	5.9	23.7	10.4
In/CuZn-350	46	0.11	7.6	7.8	20.1	9.1
Zr/CuZn-350	48	0.11	7.4	8.1	21.8	9.8
CuZr-350	73	0.18	7.9	7.8	21.3	–
CuInZr-350	77	0.18	8.8	8.2	21.7	–
In/CuZr-350	63	0.15	9.2	8.8	22.2	–
Zn/CuZr-350	61	0.15	7.8	8.7	21.9	–

CuZn-350 ($46 \text{ m}^2/\text{g}$) and Zr/CuZn-350 ($48 \text{ m}^2/\text{g}$) compared to In/CuZr-350 ($63 \text{ m}^2/\text{g}$) and Zn/CuZr-350 ($61 \text{ m}^2/\text{g}$).

3.1.2. XRD

Fig. 1 shows the XRD patterns of the CuZn, CuZr, and CuZrIn catalyst precursors. It can be seen that the diffraction patterns are in excellent agreement with the reference pattern of crystalline malachite (PDF #41–1390). For the CuZn sample, the shift of the $20\bar{1}$ ($\sim 31.5^\circ 2\theta$) and the $21\bar{1}$ ($\sim 32.5^\circ 2\theta$) peaks towards higher angles is due to Zn^{2+} incorporation into the malachite structure (Behrens et al., 2009). No shift in the position of the peaks is observed for the other precipitated samples. The presence of In ($\sim 0.3 \text{ mol}\%$) in the CuZrIn sample results in less intense and broader reflections compared to CuZr. This suggests that In is highly dispersed and prevents the crystallite growth of the malachite phase.

The XRD patterns of the calcined CuZn-350, In/CuZn-350, and Zr/CuZn-350 catalysts are shown in Fig. 2a, while Fig. 2b shows the patterns of the CuZr-350, CuZrIn-350, In/CuZr-350, and Zn/CuZr-350 catalysts. It can be seen that all of the calcined samples contain well-crystalline CuO (PDF #48–1548) with reflections at 2θ of 32.5° , 35.5° , 38.7° , and 48.7° . The CuO crystallite sizes estimated by the Scherrer equation are summarized in Table 2. The CuO crystallite size increases slightly for the impregnated catalysts, which is probably due to the second calcination cycle. Furthermore, peaks corresponding to ZnO are present for the In/CuZn-350 and Zr/CuZn-350 samples with reflections at 31.8° and 56.6° (#36–1451). On the other hand, no reflections corresponding to In_2O_3 or ZrO_2 are present in the XRD patterns, which suggests that these species are amorphous or highly dispersed.

Fig. 3a shows the XRD pattern of the CuZn-350, In/CuZn-350, and Zr/CuZn-350 catalysts after reduction at 350°C . The diffrac-

tograms of the reduced CuZr-350, CuZrIn-350, In/CuZr-350, and Zn/CuZr-350 catalysts are shown in Fig. 3b. The patterns of all the reduced catalysts show reflections at 43.3° , 50.4° , 74.1° , and 89.9° , which correspond to metallic Cu (PDF #04–0836). The crystallite size of Cu is relatively similar for the CuZn-based and CuZr-based catalysts between 20.1 and 23.7 nm (Table 2). For the CuZn catalysts, the peaks corresponding to ZnO can be observed at 31.8° , 34.4° , and 36.3° (PDF #36–1451). On the other hand, ZrO_2 seems to be amorphous, which is in agreement with literature (Tada et al., 2018b). The XRD pattern of the reduced CuIn-350 sample is shown in Figure S2c. It was found that the peaks of Cu are shifted towards lower diffraction angles for the CuIn-350 sample, which is attributed to the incorporation of In into the bulk of the Cu crystallites. Furthermore, peaks matching fairly well with that of Cu_7In_3 (PDF #65–2249) was observed, whereas crystalline In_2O_3 was not detected. To assess the migration of In into the bulk of Cu for the In-containing catalysts, the d -spacing was calculated from the Cu (311) peak (Fig. 3c). The d -spacing increases when In is impregnated onto the CuZn-350 catalyst. Interestingly, In does not appear to migrate into the bulk of Cu when In is impregnated onto the CuZr-350 catalyst, which suggests that ZrO_2 stabilizes the In oxide species. The higher d -spacing of the CuZn-based catalysts might also be related to distortion of the Cu lattice by Zn (Günter et al., 2001).

3.1.3. TGA

The TGA coupled with DSC study results of the CuZn, CuZr, and CuZrIn precursors are shown in Fig. 4a–c. The first segment below ca. 110°C and the mass loss between ca. 200 – 280°C on the TG curves correspond to the desorption of adsorbed water on the surface and loss of lattice hydroxyl groups, respectively. The significant mass loss between ca. 300 – 350°C is attributed to the decomposition of the malachite phase. An additional mass loss step centered at ca. 420°C can be observed for the CuZn precursor, which is reported to be due to carbonate decomposition and is often referred to as “high-temperature carbonate” (Kondrat et al., 2018; Kondrat et al., 2016; Tarasov et al., 2014). The higher decomposition temperature of this carbonate species for the CuZn sample is due to the incorporation of Zn into the malachite phase, as indicated by XRD. For the Zr-containing precursors, an exothermic peak can be observed at 627°C , which is ascribed to the transformation of t - ZrO_2 to m - ZrO_2 (Tada et al., 2018b). The TGA and DSC curves of the CuIn precursor is shown in Figure S3 and are similar to that of the CuZn, CuZr, and CuZrIn samples.

3.1.4. TEM

Fig. 5 shows representative TEM images of the reduced (a) CuZn-350 and (b) In/CuZn-350 catalysts. It can be seen that the morphology of CuZn-350 and In/CuZn-350 is similar. This is consistent with the comparable Cu and ZnO crystallite size of these catalysts, as indicated by XRD. A range of different particle sizes can be observed for all the samples. Several large particles and agglomerates are present, and these particles are primarily composed of Cu. The smaller particles are probably ZnO, which is supported

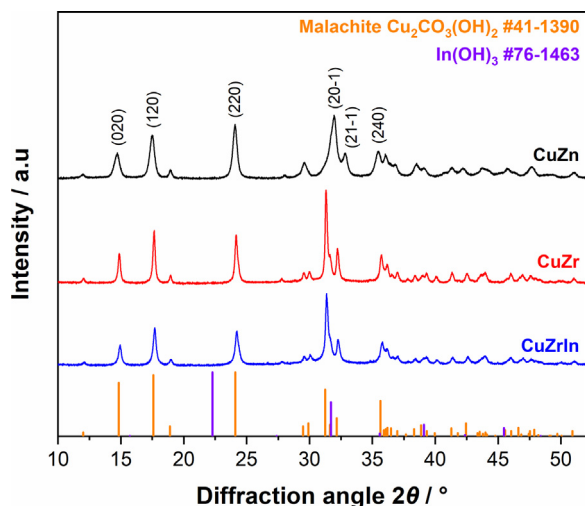


Fig. 1. XRD patterns of the CuZn, CuZr, and CuZrIn precursors prepared by coprecipitation.

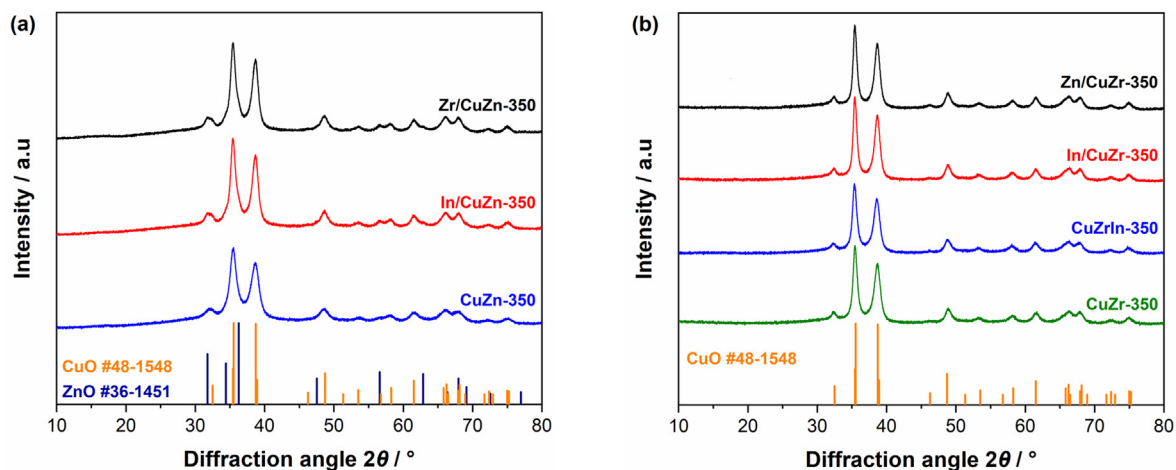


Fig. 2. XRD patterns of calcined (a) CuZn-350, In/CuZn-350, and Zr/CuZn-350; and (b) CuZr-350, CuZrIn-350, In/CuZr-350, and Zn/CuZr-350.

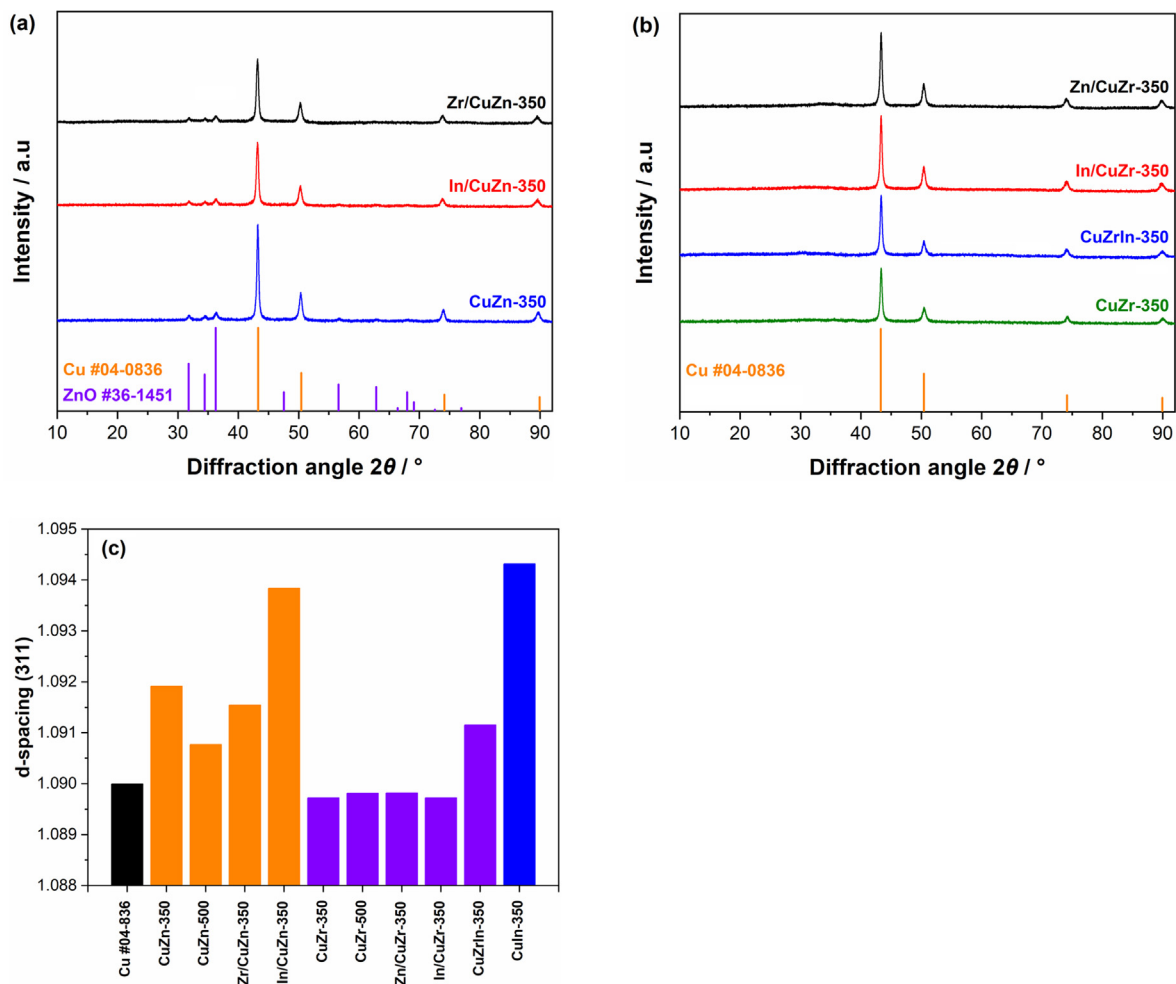


Fig. 3. XRD patterns of reduced-passivated (a) CuZn-350, In/CuZn-350, and Zr/CuZn-350; and (b) CuZr-350, CuZrIn-350, In/CuZr-350, and Zn/CuZr-350; The d-spacing of the Cu(311) peak of the reduced CuZn and CuZr catalysts (c).

by the smaller crystallite size of ZnO compared to Cu (Table 2). This is also consistent with literature (Van Den Berg et al., 2016), and one of the roles of ZnO is to act as a spacer to help disperse the Cu phase. No new features can be detected in the TEM images due to the presence of In for the In/CuZn-350 catalyst.

Fig. 6 shows the TEM images of the reduced (a) CuZr-350, (b) CuZrIn-350, and (c) In/CuZr-350 catalysts. It can be seen that dense and less dense areas are present in all of the samples. This demonstrates that ZnO is a more suitable structural promoter compared to ZrO₂. Additional TEM images comparing the morphology of

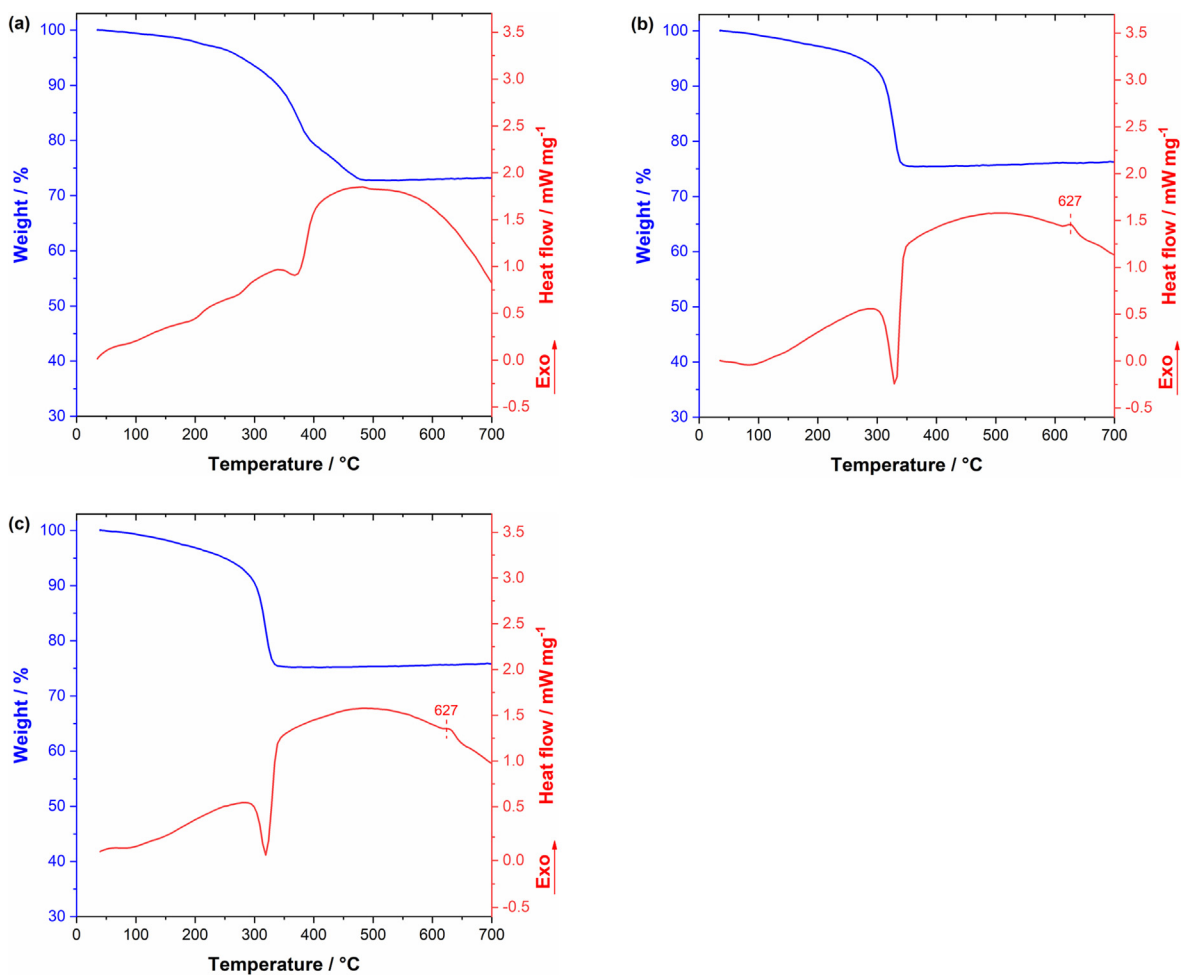


Fig. 4. TG and DSC curves for the (a) CuZn, (b) CuZr, and (c) CuZrIn precursors. Blue and red lines are the TG and DSC curves, respectively. Heating rate: 10 °C/min. (For interpretation of the references to colour in this figure legend, the reader is referred to the web version of this article.)

CuZn-350 and CuZr-350 is shown in Figure S4a and Figure S4b, respectively. The denser regions are probably arise because of the significantly smaller size of ZrO_2 compared to ZnO. This results in the Cu particles being in closer proximity to each other and can agglomerate more easily. The ZrO_2 species in the CuZr catalysts are composed of particles around 5 nm (Fig. 6d), and their size is not affected by the preparation history of the catalysts. For all the CuZr catalysts, ZrO_2 -rich and ZrO_2 -deficient areas can be identified. Thus, the ZrO_2 coverage of Cu ranges from fully covered Cu species to practically uncovered ones. No information about the

In species can be deduced from the TEM images of the In/CuZr-350 and CuZrIn-350 catalysts.

3.1.5. Reducibility of the catalysts

The deconvoluted TPR patterns of CuZn-350, In/CuZn-350, and Zr/CuZn-350 catalysts are shown in Fig. 7. Three deconvoluted peaks are identified, namely α , β , and γ , related to different CuO species. For the CuZn-350 catalysts, the reduction peaks corresponding to β - and γ -species can be observed. The β -peak is due to the reduction of surface CuO species, while the γ -peak is

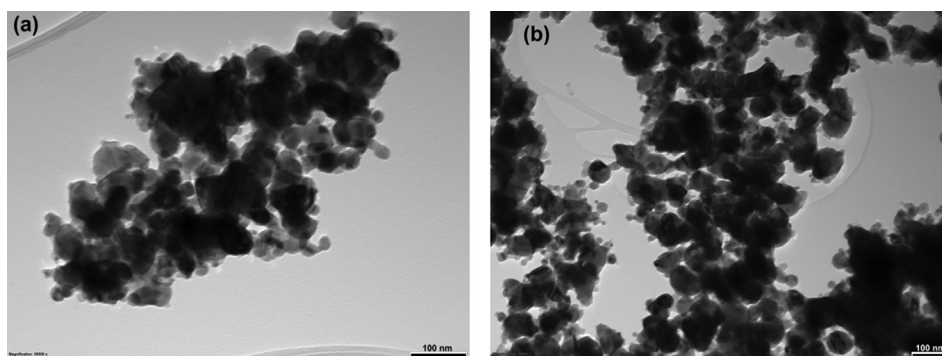


Fig. 5. TEM images of the reduced-passivated (a) CuZn-350 and (b) In/CuZn-350 catalysts.

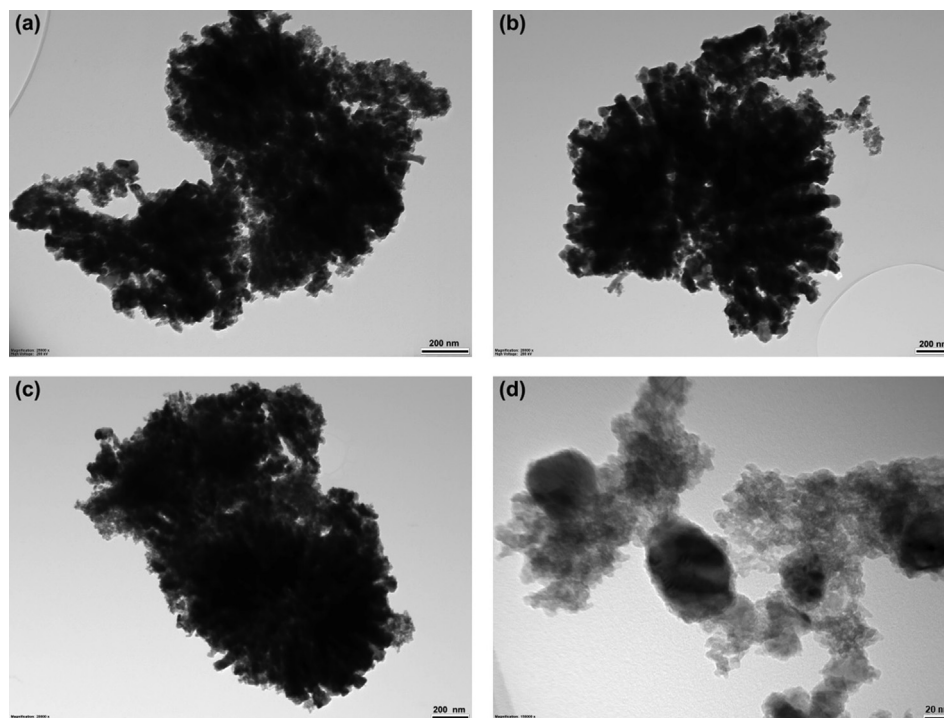


Fig. 6. TEM images of the reduced-passivated (a) CuZr-350, (b) CuZrIn-350, (c) In/CuZr-350, and (d) CuZr-350 (higher magnification) catalysts.

ascribed to the reduction of bulk CuO (Gao et al., 2012; Gao et al., 2013). The impregnation of In_2O_3 or ZrO_2 onto the CuZn-350 catalyst results in the formation of an α -peak located at a lower temperature. *In situ* X-ray adsorption near edge structure (XANES) has identified that the reduction of CuO proceeds through two steps ($\text{CuO} \rightarrow \text{Cu}_2\text{O} \rightarrow \text{Cu}$) when CuO is in intimate contact with ZnO (Kühl et al., 2014), ZnAl_2O_4 (Kühl et al., 2014), and ZrO_2 (Ro et al., 2016). In contrast to ZnO, the ZnAl_2O_4 and ZrO_2 can stabilize the Cu_2O intermediate, which results in a pronounced shoulder in the TPR pattern. The α -peak can also be observed in the TPR profile of the CuIn-350 catalyst (Figure S5). Therefore, the α -species are related to stabilized Cu_2O species formed at lower reduction temperature due to the enhanced reducibility of CuO in contact with In_2O_3 and ZrO_2 . The H_2/CuO ratios were estimated from the TPR

peak areas and are summarized in Table 3. The H_2/Cu ratio is close to 1 for CuZn catalysts, indicating complete reduction of CuO. For the CuIn-350 catalysts, the H_2/Cu ratio is 1.12 below 240 °C, indicating that highly dispersed In_2O_3 species also are reduced at relatively low temperature.

The deconvoluted TPR patterns of the CuZr-350, CuZrIn-350, In/CuZr-350, and Zn/CuZr-350 catalysts are shown in Fig. 8. It can be seen that the α -peak areas are higher for the CuZr catalysts compared to the Zr/CuZn-350 and In/CuZn-350 samples because of the higher ZrO_2 content. The incorporation of In by co-precipitation shift the reduction profile towards lower temperature, which might be due to the presence of In in the bulk of CuO. Interestingly, In/CuZr-350 contains the lowest number of α -species of the CuZr catalysts, whereas the formation α -species occurs when In is impregnated onto CuZn-350 (Table 3). The number of α -species is also reduced when Zn is impregnated onto the CuZr-350 catalysts. The lower amount of α -species suggests that In and Zn adsorption is more favorable on the ZrO_2 phase during impregnation, which reduces the interaction between Cu and ZrO_2 . The H_2/Cu ratio is 0.92 and 0.93 for the CuZr-350 and In/CuZr-350, respectively, which could be due to the formation of stable Cu^+ species. On the other hand, the H_2/Cu ratio is close to 1 for the CuZrIn-350 and Zn/CuZr-350 catalysts.

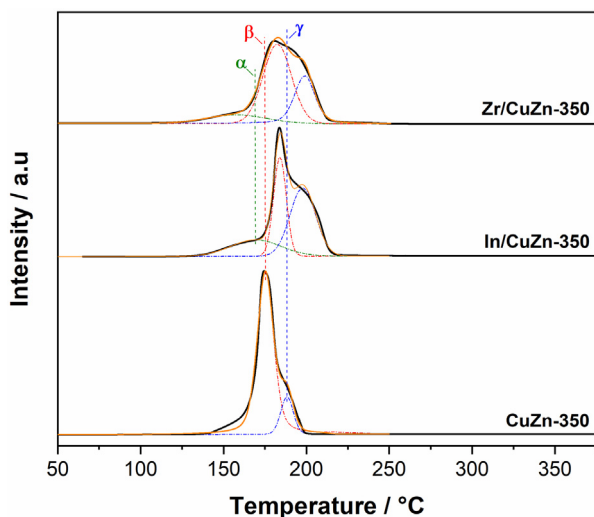


Fig. 7. Deconvoluted H_2 -TPR patterns of the CuZn-350, In/CuZn-350, and Zr/CuZn-350 catalysts.

3.1.6. N_2O adsorption measurements

The Cu surface areas were estimated by N_2O adsorption and are summarized in Table 3. The Cu surface area of the CuZn-350 is $18 \text{ m}^2/\text{g}$, which decreases to $14 \text{ m}^2/\text{g}$ when In is impregnated onto the CuZn-350 catalyst. On the other hand, the Cu surface area of the Zr/CuZn-350 catalyst ($17 \text{ m}^2/\text{g}$) is comparable to that of CuZn-350. The smaller number of Cu atoms on the surface of In/CuZn-350 is attributed to In-migration onto the Cu surface during reduction. This is supported by the significant drop in Cu surface area when the reduction temperature is increased for the CuIn-350 catalyst (Figure S6). The CuZr-350, CuZrIn-350, and Zn/CuZr-350 catalysts exhibit similar Cu surface areas in the range

Table 3Summary of H₂-TPR results, Cu surface areas, and relative number of MB sites of the CuZn and CuZr catalysts.

Catalyst	H ₂ /CuO ratio	α (%) ^a	β (%) ^a	γ (%) ^a	SA _{Cu} (m ² /g) ^b	Relative number of MB sites	A _{HT-MB} /A _{MB}
CuZn-350	0.98 ^a	0	85.5	15.5	18	0.22 ^c	0
In/CuZn-350	1.01 ^a	13.3	59.1	27.6	14	0.18 ^c	0
Zr/CuZn-350	1.00 ^a	32.9	45.8	21.3	17	0.35 ^c	0
CuZr-350	0.92 ^a	38.1	48.9	13.0	34	1.00 ^c	0.24 ^d
CuZrIn-350	0.99 ^a	37.7	37.0	25.3	36	0.86 ^c	0.42 ^d
In/CuZr-350	0.93 ^a	26.1	40.2	33.7	26	0.55 ^c	0.35 ^d
Zn/CuZr-350	0.98 ^a	29.1	49.5	21.4	32	0.88 ^c	0.26 ^d

^a Determined from H₂-TPR.^b Estimated from N₂O chemisorption.^c Obtained from CO₂-TPD; ^d Ratio of high-temperature MB sites to total number of MB sites.

of 31–36 m²/g. It can be seen that the Cu surface area is also significantly reduced when In is impregnated onto the CuZr-350 catalyst (26 m²/g). It has been reported that the oxygen vacancies of metal oxides can contribute to the N₂O consumption (Chatterjee et al., 2019; Fichtl et al., 2014; Kuld et al., 2014). Nevertheless, the decrease in Cu surface area is relatively high when In is impregnated onto CuZn-350 and CuZr-350, which suggests that the Cu surface is partially covered by In after reduction for both catalysts.

3.1.7. CO₂-TPD

The surface basicity of the catalysts was studied by CO₂-TPD. Fig. 9a shows the CO₂-TPD profiles of CuZn-350, In/CuZn-350, and Zr/CuZn-350, while the profiles of CuZr-350, CuZrIn-350, In/CuZr-350, and Zn/CuZr-350 are shown in Fig. 9b. The profiles were deconvoluted into three regions: weak basic (WB) sites related to the Cu surface (Bönnicke et al., 1994) or OH⁻ groups (50–200 °C), medium-strength basic (MB) sites associated with metal–oxygen pairs (e.g., Zr–O, In–O) (200–480 °C), and strong basic sites due to low-coordination O²⁻ species (480–800 °C) (Zhang et al., 2020). The MB sites of the CuZn catalyst might be due to oxygen defects in ZnO or ZnO_x species present on the Cu surface after reduction (Zhao et al., 2018). It can be seen the number of moderate basic sites increases when ZrO₂ is impregnated onto the CuZn-350 catalyst, which is attributed to the presence of additional CO₂ adsorption sites at Lewis basic sites of ZrO₂ (Arena et al., 2008; Dong et al., 2016). Furthermore, the Zr/CuZn-350 catalyst also contains a significant amount of strong basic sites. On the other hand, the addition of In reduces the surface basicity of the CuZn-350 cat-

alyst. This indicates that In inhibits the Cu–ZnO interaction or reduces the number of oxygen defects in ZnO.

Different types of MB and SB sites are also present in the CO₂ TPD profiles of the CuZr catalysts (Fig. 9b). The CuZr-350 has the highest quantity of MB sites (Table 3). Incorporation of In by coprecipitation results in a higher fraction of high-temperature MB sites for the CuZrIn-350 catalyst. When Zn or In is impregnated onto the CuZr-350 catalyst, the amount of MB sites decreases accompanied by a significant increase in SB sites. Since the amount of SB sites is also very high for the Zr/CuZn-350 sample, the increase in SB sites for the impregnated catalysts is probably related to the interaction between ZnO or In₂O₃ species with ZrO₂.

The CO₂-TPD profiles of CuIn-350, CuZn-500, and CuZr-500 are shown in Figure S7. Notably, the surface basicity of the CuIn-350 catalyst is much lower than that of the other samples and the surface basicity is reduced when the CuZn and CuZr catalysts are calcined at 500 °C. The lower surface basicity of CuZn-500 compared to CuZn-350 might be related to a weaker Cu–ZnO interaction (Li et al., 2016). Furthermore, the number of defects and oxygen vacancies in ZnO and ZrO₂ might be lower after calcination at higher temperature.

3.2. Catalytic activity tests

3.2.1. Comparison of the CuZr and CuZn catalysts

Fig. 10 shows the steady-state production rates of methanol and CO for the CuZn and CuZr catalysts. A summary of the characterization results of the CuZn-500 and CuZr-500 catalysts can be found in the Table S1. A methanol formation rate of 14.7 mmol·g_{cat}⁻¹·h⁻¹ is obtained over the CuZn-350 catalyst. Although the CuZn-500 catalyst shows similar overall activity, a decrease in the methanol formation rate (12.4 mmol·g_{cat}⁻¹·h⁻¹) accompanied by an increase in the CO production rate can be observed. Li et al. (Li et al., 2016) observed that the amount of CuZn alloy decreases with increasing calcination temperature for the Cu/ZnO catalyst. Thus, the lower activity of CuZn-500 might be related to a lower amount of CuZn sites for CO₂ hydrogenation to methanol (Zabitskiy et al., 2020), as indicated by XRD and CO₂-TPD. The highest steady-state methanol formation rate is obtained over the Zr/CuZn-350 catalyst (15.6 mmol·g_{cat}⁻¹·h⁻¹). In fact, the initial rate of the Zr/CuZn-350 catalyst is approximately 2 times higher than CuZn-350 (Figure S8), which is in the high range of STY values previously reported in literature at comparable conditions (Table S2). Recently, Wu et al. (Wu et al., 2020) detected a HCOO–Cu intermediate over an inverse ZrO₂/Cu catalyst, which was hydrogenated to methanol at a significantly higher rate compared to formate species on ZrO₂. The increase in the number of moderate basic sites for the Zr/CuZn-350 catalysts is indicative of Cu–ZrO₂ interfacial sites, which probably have an inverse ZrO₂/Cu configuration. Thus, the superior performance of Zr/CuZn-350 is attributed to the formation of Cu–ZrO₂ interfacial sites that facilitate CO₂ hydrogenation to methanol.

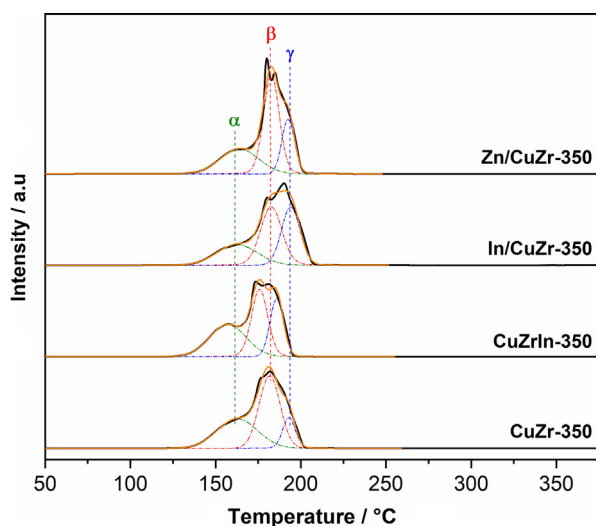


Fig. 8. Deconvoluted H₂-TPR patterns of the CuZr-350, CuZrIn-350, In/CuZr-350, and Zn/CuZr-350 catalysts.

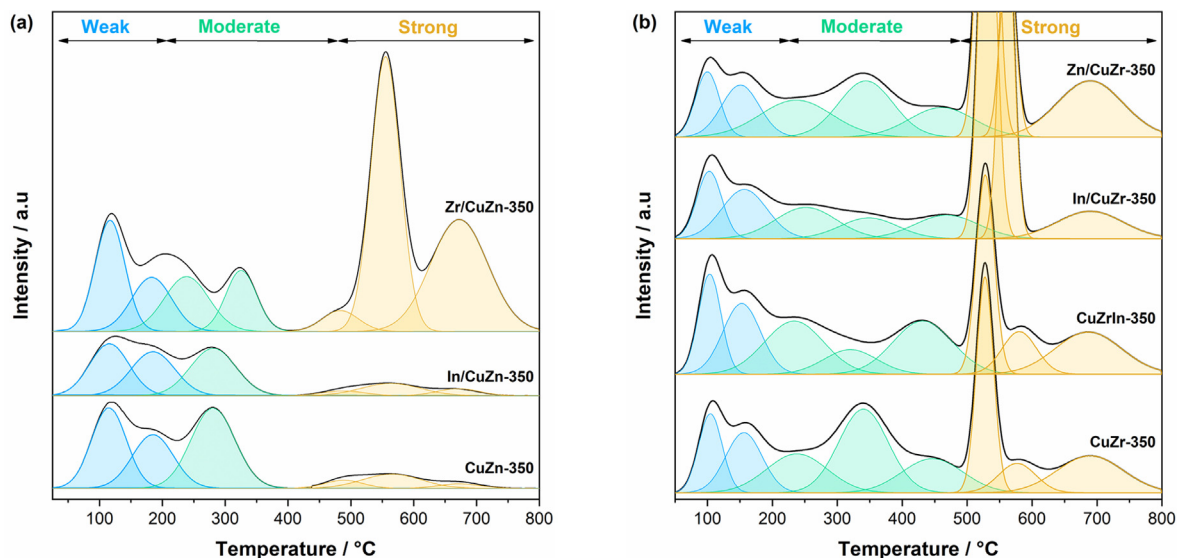


Fig. 9. CO₂-TPD profiles of the (a) CuZn-350, In/CuZn-350, and Zr/CuZn-350 catalysts; and the (b) CuZr-350, CuZrIn-350, In/CuZr-350, and Zn/CuZr-350 catalysts.

The methanol formation rate of the CuZr-350 catalyst ($13.1 \text{ mmol} \cdot \text{g}_{\text{cat}}^{-1} \cdot \text{h}^{-1}$) is lower than that of CuZn-350 despite the higher Cu surface area. The activity of Cu/ZrO₂-based catalysts is critically linked to the interfacial sites, which facilitate CO₂ activation and hydrogenation to methanol (Ro et al., 2016; Rungtaweivoranit et al., 2016; Samson et al., 2014; Tada et al., 2018b; Wang et al., 2019b). Therefore, the Cu surface area obtained from N₂O chemisorption is not a suitable descriptor of the number of active sites for the Cu/ZrO₂-based catalysts investigated in this work. Zr-rich and Zr-deficient regions are present in the TEM images of the CuZr catalysts, indicating that the employed preparation method is not optimal for obtaining well-mixed Cu/ZrO₂ catalysts. The lower activity of the CuZr-500 catalysts can be explained by the decrease in surface basicity after calcination at 500 °C, which reduces the number of sites for CO₂ activation. The activity also decreases when ZnO is impregnated onto CuZr-350. The ZnO-ZrO₂ interaction seems to generate strong basic sites, which might adsorb CO₂ or reaction intermediates too strongly for further hydrogenation to methanol.

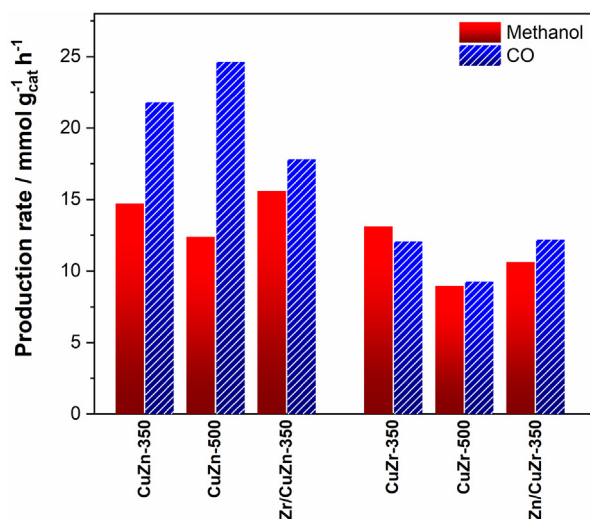


Fig. 10. Methanol and CO production rates for the CuZn and CuZr catalysts. Reaction conditions: 230 °C, 30 bar, $38\,000 \text{ cm}^3/(\text{g}_{\text{cat}} \text{ h})$, H₂/CO₂ = 3.

To compare the methanol selectivity of the CuZn and CuZr catalysts, the effect of contact time was investigated by varying the GHSV between 20 000 and 100 000 $\text{cm}^3 \cdot \text{g}_{\text{cat}}^{-1} \cdot \text{h}^{-1}$. The methanol selectivity is plotted against the CO₂ conversion after reaching stable production rates for the CuZn and CuZr catalyst in Fig. 11a and b, respectively. The methanol selectivity increases with decreasing CO₂ conversion, i.e., increasing GHSV, for all the catalysts in accordance with literature (Tada et al., 2018b). Extrapolation of the methanol selectivity to zero conversion (zero contact time) of the CuZn and CuZr catalysts yields a positive initial formation rate for both methanol and CO. This indicates that methanol and CO are primary products over the CuZn and CuZr catalysts (Larmier et al., 2017). The shape and location of the trend lines are related to the active sites present on the catalysts' surface. The active sites of CuZn-350 and CuZn-500 can generally be divided into (i) surface metallic Cu and (ii) Cu-ZnO interfacial sites. The methanol selectivity of CuZn-350 and CuZn-500 indicates that CO formation rate increases with weaker Cu-ZnO interaction. Thus, the unpromoted Cu surface seem to be more active for the RWGS reaction. The increase in methanol selectivity when Zr is impregnated onto CuZn-350 is probably due to the additional Cu-ZrO₂ interfacial sites.

It can be seen in Fig. 11b that the methanol selectivity is significantly higher for the CuZr-350 catalysts compared to CuZr-500. Generally, three types of active sites are probably present for these catalysts, namely (i) surface metallic Cu, (ii) Cu/*a*-ZrO₂, and (iii) Cu/*t*-ZrO₂. It has been reported that the methanol synthesis activity of Cu supported on *a*-ZrO₂ is higher than that of *t*-ZrO₂ (Tada et al., 2018b). Therefore, the lower methanol selectivity of CuZr-500 might be related to the transformation of *a*-ZrO₂ into *t*-ZrO₂, as indicated by XRD (Figure S2d). Based on the CO₂-TPD results, the number of CO₂ adsorption sites decreases when the catalyst is calcined at higher temperature, reducing the number of sites for CO₂ activation. The methanol selectivity is also lower for Zn/CuZr-350 compared to CuZr-350.

3.2.2. Influence of *in* on CuZn and CuZr catalysts

The steady-state methanol formation rates of the CuZn-350*, In/CuZn-350, CuZr-350, CuZr-350*, CuZrIn-350, and In/CuZr-350 catalysts at 230 °C and 270 °C are shown in Fig. 12. A significant decrease in the methanol formation rate is observed when In is impregnated onto the CuZn-350 and CuZr-350 catalysts. The

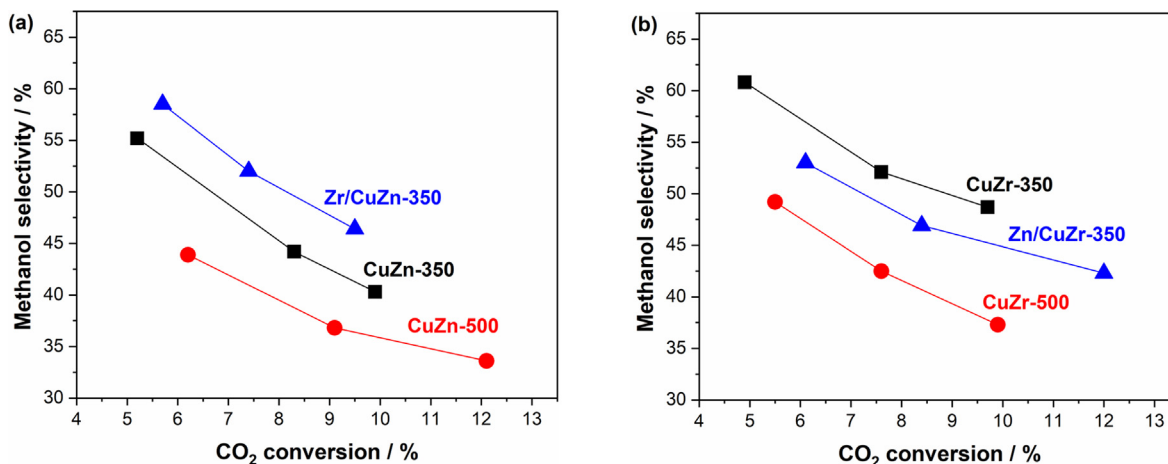


Fig. 11. Methanol selectivity as a function of CO₂ conversion for (a) CuZn-350, CuZn-500, and Zr/CuZn-350; and (b) CuZr-350, CuZr-500, and Zn/CuZr-350 catalysts. Reaction conditions: 230 °C, 30 bar, H₂/CO₂ = 3.

activity of the CuIn-350 catalyst was negligible at 270 °C (see Table S1 for summary of characterization results of CuIn-350). Thus, the significant decrease in Cu surface area indicates that In coverage of the active sites is responsible for the lower activity for the In/CuZn-350 catalyst. The CO₂-TPD results suggests that the blockage of MB sites of CuZr-350 reduces the activity of the catalyst. Interestingly, the methanol formation rate of CuZrIn-350 is clearly higher than that of CuZr-350 at 270 °C. The ratio of high-temperature MB sites to the total amount of MB sites (A_{HT-MB}/A_{MB} , Table 3) is higher for CuZrIn-350 and In/CuZr-350 compared to the CuZr-350, Zn/CuZr-350, and CuZr-500 (Table S1) catalysts. This shift in the basic site composition might be related to the presence of In-Zr mixed oxide sites. Typically, In₂O₃ and ZrO₂-promoted In₂O₃ catalysts are reported to require higher temperatures than Cu/ZnO and Cu/ZrO₂ to achieve significant methanol synthesis activity (Chou and Lobo, 2019; Dang et al., 2020; Frei et al., 2019; Martin et al., 2016). Therefore, the superior activity of CuZrIn-350 at 270 °C might be related to the contribution of In-Zr mixed oxide sites that are not particularly active at 230 °C.

The methanol selectivity as a function of CO₂ conversion is plotted for the CuZn-350*, In/CuZn-350, CuZr-350*, CuZrIn-350, and In/

CuZr-350 catalysts at 230 °C and 270 °C in Fig. 13a and b, respectively. It can be seen that the trend curves appear at higher methanol selectivity when In is impregnated onto the CuZn-350 and CuZr-350 catalysts at both temperatures. For the CuZrIn-350 catalyst, the methanol selectivity is higher than that of the CuZr-350* catalyst only at 270 °C. Furthermore, the methanol selectivity is more significantly improved for In/CuZr-350 and CuZrIn-350 compared to In/CuZn-350 when the reaction temperature is increased. Therefore, In addition to the catalysts might improve the methanol selectivity in two different ways: (i) by decreasing the number of metallic Cu sites for the RWGS reaction by forming Cu_xIn_y surface species; and (ii) generating In-Zr mixed oxide sites for methanol synthesis. For the In/CuZn-350 catalyst, the methanol selectivity is probably improved due to a decrease in metallic Cu sites, whereas a combination of (i) and (ii) explains the performance of the In/CuZr-350 catalyst. On the other hand, the selectivity of the CuZrIn-350 catalyst indicate a negligible fraction of Cu_xIn_y surface species. This is probably due to the lower In content and a consequence of the preparation method, which leads to In being mostly incorporated into the bulk of Cu and the ZrO₂ phase. It is also likely that this enhances the stability of the Cu and ZrO₂ phases, which limits the deactivation at 270 °C (Figure S9).

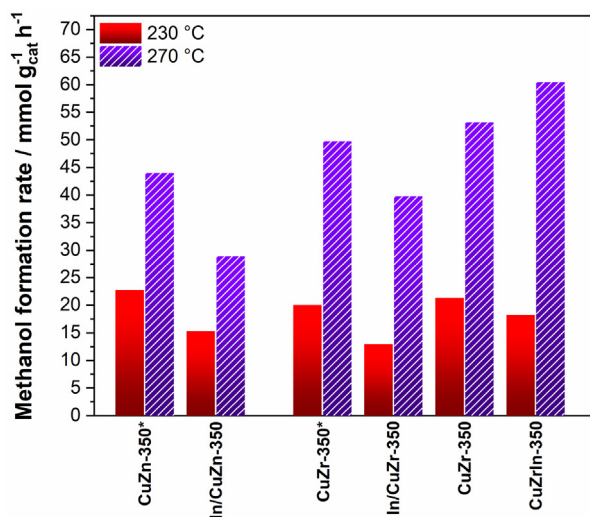


Fig. 12. Methanol formation rates for the CuZn-350*, In/CuZn-350, CuZr-350, CuZr-350*, CuZrIn-350, and In/CuZr-350 catalysts. Reaction conditions: 230 °C, 30 bar, 80 000 cm³/(g_{cat} h), H₂/CO₂ = 3 and 270 °C, 30 bar, 140 000 cm³/(g_{cat} h), H₂/CO₂ = 3.

3.2.3. Influence of surface properties on catalytic performance

Fig. 14a shows the STY of methanol as a function of the Cu surface area. The Cu surface areas of the CuZn-500, CuZn-350, and Zr/CuZn-350 are comparable, but their activity is drastically different. Furthermore, the CuZr-based catalysts exhibit much lower STY of methanol per Cu surface area compared to the CuZn-based catalysts. The decoration of the Cu surface by Zn or ZnO_x species has been reported to yield a highly abundant Cu-ZnO interface for the conversion of CO₂ to methanol (Behrens et al., 2012; Kuld et al., 2014; Kattel et al., 2016; Zabilskiy et al., 2020). Therefore, the ability of Zn species to incorporate into the Cu precursor phase has probably resulted in a larger Cu-oxide interface for the CuZn-based catalysts. On the other hand, the STY of CO strongly correlates to the Cu surface area (Fig. 14b), indicating that CO formation primarily occurs on the Cu surface. According to literature (Grabow, 2011; Graciani et al., 2014; Kattel et al., 2016), CO formation occurs through the carboxyl (COOH) intermediate rather than the decomposition of formate (HCOO). The reaction mechanism over Cu/ZrO₂-based catalysts has been debated, where both direct hydrogenation of CO₂ via the formate intermediate and methanol formation via CO as an intermediate has been proposed (Li and Chen, 2019). Thus, further hydrogenation of CO formed from the

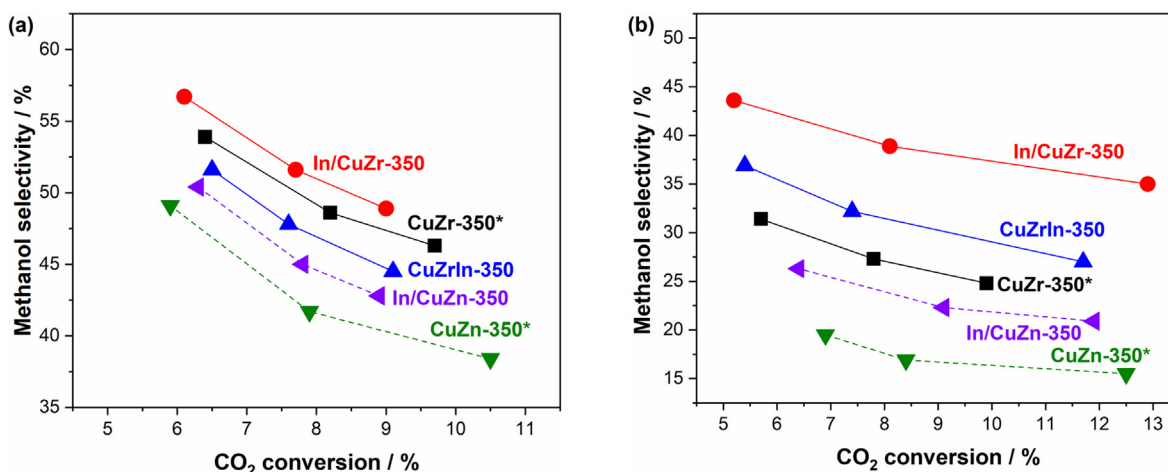


Fig. 13. Methanol selectivity as a function of CO₂ conversion for the CuZn-350*, In/CuZn-350, CuZr-350*, CuZrIn-350, and In/CuZr-350 catalysts at (a) 230 °C and (b) 270 °C. Reaction conditions: 30 bar, H₂/CO₂ = 3.

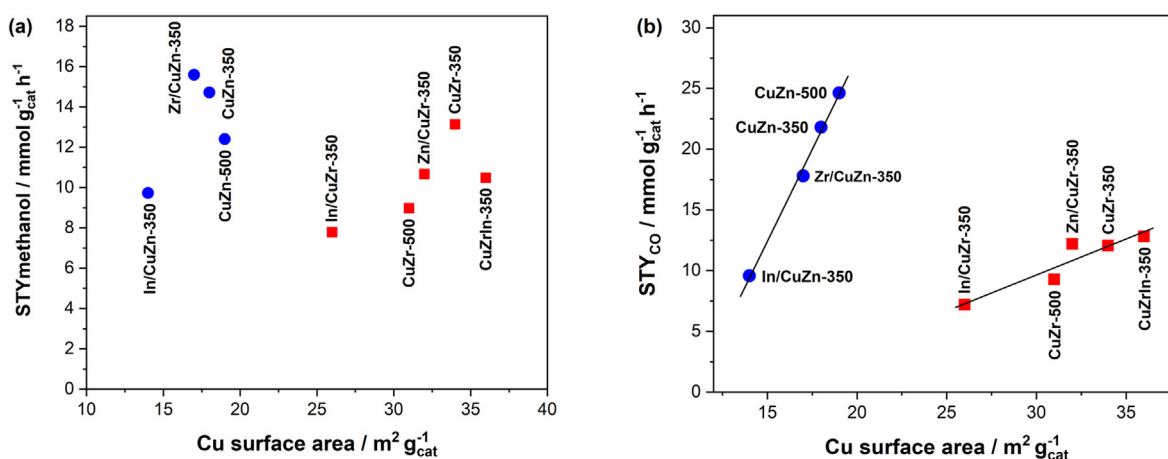


Fig. 14. STY of methanol (a) and CO (b) at 230 °C as a function of Cu surface area for the CuZn and CuZr catalysts.

RWGS reaction might also contribute to the methanol production when ZrO₂ is present.

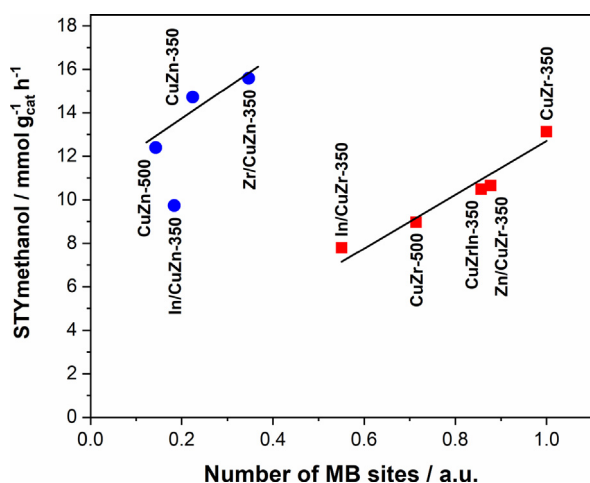


Fig. 15. STY of methanol at 230 °C as a function of the relative number of MB sites for the CuZn and CuZr catalysts.

The STY of methanol as a function of the relative number of MB sites is shown in Fig. 15. A correlation between the methanol formation rate and the number of MB sites can be observed with the exception of the In/CuZn-350 catalyst. The basicity of Cu-based catalysts has been reported to be an important factor for the methanol synthesis activity of Cu-based catalysts (Gao et al., 2013; Gao et al., 2016; Guo et al., 2011; Wang et al., 2019a). Thus, the results indicate that the number of interfacial sites is reflected by the MB sites and is an important descriptor of the methanol synthesis activity over these catalysts. The number of SB sites is significantly higher for the impregnated Zr/CuZn-350, Zn/CuZr-350, and In/CuZr-350 catalysts. However, these adsorption sites seem to bind CO₂ or CO₂ derived species too strongly for further hydrogenation and not contribute to the activity of the catalyst. The very high initial methanol formation rate of Zr/CuZn-350 compared to the CuZn-350, CuZr-350 and Zn/CuZr-350 catalysts demonstrates that obtaining high coverage of the Cu surface of Zn(O) and ZrO₂ species can significantly boost the methanol production.

4. Conclusion

The model catalysts investigated in this work provide insights into the generation and inhibition of active sites of Cu-based

catalysts for CO₂ hydrogenation. The impregnation of a small amount of ZrO₂ onto Cu/ZnO significantly improves the methanol selectivity of the catalyst. Furthermore, the initial methanol formation rate is approximately two times higher for the ZrO₂-containing Cu/ZnO catalyst. The introduction of ZrO₂ generates new medium-strength basic sites for CO₂ activation and conversion to methanol. However, the catalyst deactivates rapidly, but the steady-state methanol selectivity and methanol formation rate (15.6 mmol/gcat) are still higher than the unpromoted Cu/ZnO catalyst (14.7 mmol/gcat). In contrast, when ZnO is impregnated onto Cu/ZrO₂, both the methanol selectivity and methanol formation rate are reduced. This is attributed to the formation of CO₂ adsorption sites that bind the CO₂-derived species too strongly for further hydrogenation to methanol, which reduces the number of active Cu-oxide interfacial sites.

We also demonstrate that In can inhibit the RWGS reaction on the Cu/ZnO and Cu/ZrO₂ catalysts. The results suggest that inactive Cu_xIn_y surface species are formed that block CO production on the Cu surface. Furthermore, the methanol formation rate increases from 52.7 to 60.5 mmol/g_{cat} at 270 °C when 0.3 mol% In is incorporated into the Cu/ZrO₂ catalyst by co-precipitation. The higher activity of In-doped Cu/ZrO₂ is attributed to In-Zr mixed oxide sites that are more active for methanol synthesis at higher temperatures. Furthermore, In improves the stability of the catalyst, which is attributed to the presence of In in the bulk of Cu and in the ZrO₂ phase that stabilizes the interfacial sites. The present findings provide insight into tuning the active sites and enhancing the stability of Cu-based catalyst promoted by metal oxides for CO₂ hydrogenation to methanol.

CRediT authorship contribution statement

Kristian Stangeland: Conceptualization, Investigation, Writing - original draft. **Hans Herrera Navarro:** Investigation, Resources. **Huong Lan Huynh:** Investigation. **Wakshum Mekonnen Tucho:** Investigation. **Zhixin Yu:** Supervision, Writing - review & editing.

Declaration of Competing Interest

The authors declared that there is no conflict of interest.

Acknowledgements

The authors would like to thank the financial support from the Norwegian Ministry of Education and Research and the Department of Energy and Petroleum Engineering, University of Stavanger for this project.

Appendix A. Supplementary data

Supplementary data to this article can be found online at <https://doi.org/10.1016/j.ces.2021.116603>.

References

- Arena, F., Italiano, G., Barbera, K., Bordiga, S., Bonura, G., Spadaro, L., Frusteri, F., 2008. Solid-state interactions, adsorption sites and functionality of Cu-ZnO/ZrO₂ catalysts in the CO₂ hydrogenation to CH₃OH. *Appl. Catal. A* 350, 16–23. <https://doi.org/10.1016/j.apcata.2008.07.028>.
- Aresta, M., Dibenedetto, A., Quaranta, E., 2016. State of the art and perspectives in catalytic processes for CO₂ conversion into chemicals and fuels: The distinctive contribution of chemical catalysis and biotechnology. *J. Catal.* 343, 2–45. <https://doi.org/10.1016/j.jcat.2016.04.003>.
- Baiker, A., Kilo, M., Maciejewski, M., Menzi, S., Wokaun, A., 1993. Hydrogenation of CO₂ over copper, silver and gold/zirconia catalysts: Comparative study of catalyst properties and reaction pathways. *Studies in Surface Science and*

- Catalysis*. Elsevier, 1257–1272. [https://doi.org/10.1016/S0167-2991\(08\)64449-3](https://doi.org/10.1016/S0167-2991(08)64449-3).
- Behrens, M., Girgsdies, F., Trunschke, A., Schlögl, R., 2009. Minerals as model compounds for Cu/ZnO catalyst precursors: structural and thermal properties and IR spectra of mineral and synthetic (zincian) malachite, rosasite and aurichalcite and a catalyst precursor mixture. *Eur. J. Inorg. Chem.* 2009, 1347–1357. <https://doi.org/10.1002/ejic.200801216>.
- Behrens, M., Schlögl, R., 2013. How to prepare a good Cu/ZnO catalyst or the role of solid state chemistry for the synthesis of nanostructured catalysts. *Zeitschrift für anorganische und allgemeine Chemie* 639, 2683–2695. <https://doi.org/10.1002/zaac.201300356>.
- Behrens, M., Studt, F., Kasatkin, I., Kühl, S., Hävecker, M., Abild-Pedersen, F., Zander, S., Girgsdies, F., Kurr, P., Knief, B.-L., 2012. The active site of methanol synthesis over Cu/ZnO/Al₂O₃ industrial catalysts. *Science* 336, 893–897. <https://doi.org/10.1126/science.1219831>.
- Bönicke, I.A., Kirstein, W., Thieme, F., 1994. A study on CO₂ dissociation on a stepped (332) copper surface. *Surf. Sci.* 307, 177–181. [https://doi.org/10.1016/0039-6028\(94\)90390-5](https://doi.org/10.1016/0039-6028(94)90390-5).
- Chatterjee, R., Kuld, S., van den Berg, R., Chen, A., Shen, W., Christensen, J.M., Jensen, A.D., Sehested, J., 2019. Mapping support interactions in copper catalysts. *Top. Catal.* 62, 649–659. <https://doi.org/10.1007/s11244-019-01150-9>.
- Chen, K., Fang, H., Wu, S., Liu, X., Zheng, J., Zhou, S., Duan, X., Zhuang, Y., Tsang, S.C.E., Yuan, Y., 2019. CO₂ hydrogenation to methanol over Cu catalysts supported on La-modified SBA-15: The crucial role of Cu-LaO_x interfaces. *Appl. Catal. B* 251, 119–129. <https://doi.org/10.1016/j.apcatb.2019.03.059>.
- Chou, C.-Y., Lobo, R.F., 2019. Direct conversion of CO₂ into methanol over promoted indium oxide-based catalysts. *Appl. Catal. A* 583. <https://doi.org/10.1016/j.apcata.2019.117144>.
- Dang, S., Qin, B., Yang, Y., Wang, H., Cai, J., Han, Y., Li, S., Gao, P., Sun, Y., 2020. Rationally designed indium oxide catalysts for CO₂ hydrogenation to methanol with high activity and selectivity. *Science. Advances* 6, eaaz2060. <https://doi.org/10.1126/sciadv.aaz2060>.
- Denise, B., Sneed, R., 1986. Oxide-supported copper catalysts prepared from copper formate: Differences in behavior in methanol synthesis from CO/H₂ and CO₂/H₂ mixtures. *Applied Catalysis* 28, 235–239. [https://doi.org/10.1016/S0166-9834\(00\)82507-5](https://doi.org/10.1016/S0166-9834(00)82507-5).
- Dong, X., Li, F., Zhao, N., Xiao, F., Wang, J., Tan, Y., 2016. CO₂ hydrogenation to methanol over Cu/ZnO/ZrO₂ catalysts prepared by precipitation-reduction method. *Appl. Catal. B* 191, 8–17. <https://doi.org/10.1016/j.apcatb.2016.03.014>.
- Fichtl, M.B., Schumann, J., Kasatkin, I., Jacobsen, N., Behrens, M., Schlögl, R., Muhler, M., Hinrichsen, O., 2014. Counting of oxygen defects versus metal surface sites in methanol synthesis catalysts by different probe molecules. *Angew. Chem. Int. Ed.* 53, 7043–7047. <https://doi.org/10.1002/anie.201400575>.
- Frei, M.S., Mondelli, C., García-Muelas, R., Kley, K.S., Puértolas, B., López, N., Safonova, O.V., Stewart, J.A., Ferré, D.C., Pérez-Ramírez, J., 2019. Atomic-scale engineering of indium oxide promotion by palladium for methanol production via CO₂ hydrogenation. *Nat. Commun.* 10. <https://doi.org/10.10961/iochem-bd-1-106>. 1–11.
- Fujitani, T., Nakamura, I., Uchijima, T., Nakamura, J., 1997a. The kinetics and mechanism of methanol synthesis by hydrogenation of CO₂ over a Zn-deposited Cu(111) surface. *Surf. Sci.* 383, 285–298. [https://doi.org/10.1016/S0039-6028\(97\)00192-1](https://doi.org/10.1016/S0039-6028(97)00192-1).
- Fujitani, T., Nakamura, I., Ueno, S., Uchijima, T., Nakamura, J., 1997b. Methanol synthesis by hydrogenation of CO₂ over a Zn-deposited Cu(111): formate intermediate. *Appl. Surf. Sci.* 121, 583–586. [https://doi.org/10.1016/S0169-4332\(97\)00372-3](https://doi.org/10.1016/S0169-4332(97)00372-3).
- Fujiwara, K., Tada, S., Honma, T., Sasaki, H., Nishijima, M., Kikuchi, R., 2019. Influences of particle size and crystallinity of highly loaded CuO/ZrO₂ on CO₂ hydrogenation to methanol. *AIChE J.* 65. <https://doi.org/10.1002/aic.16717> e16717.
- Gao, J., Song, F., Li, Y., Cheng, W., Yuan, H., Xu, Q., 2020. Cu₂In nanoalloy enhanced performance of Cu/ZrO₂ catalysts for the CO₂ hydrogenation to methanol. *Industrial Engineering Chemistry Research*. <https://doi.org/10.1021/acs.iecr.9b06956>.
- Gao, P., Li, F., Xiao, F., Zhao, N., Sun, N., Wei, W., Zhong, L., Sun, Y., 2012. Preparation and activity of Cu/Zn/Al/Zr catalysts via hydrotalcite-containing precursors for methanol synthesis from CO₂ hydrogenation. *Catalysis Science Technology* 2, 1447–1454. <https://doi.org/10.1039/C2CY00481J>.
- Gao, P., Li, F., Zhao, N., Xiao, F., Wei, W., Zhong, L., Sun, Y., 2013. Influence of modifier (Mn, La, Ce, Zr and Y) on the performance of Cu/Zn/Al catalysts via hydrotalcite-like precursors for CO₂ hydrogenation to methanol. *Appl. Catal. A* 468, 442–452. <https://doi.org/10.1016/j.apcata.2013.09.026>.
- Gao, P., Yang, H., Zhang, L., Zhang, C., Zhong, L., Wang, H., Wei, W., Sun, Y., 2016. Fluorinated Cu/Zn/Al/Zr hydrotalcites derived nanocatalysts for CO₂ hydrogenation to methanol. *J. CO₂ Utilization* 16, 32–41. <https://doi.org/10.1016/j.jcou.2016.06.001>.
- Gaikwad, R., Reymond, H., Phongprueksathat, N., von Rohr, P.R., Urakawa, A., 2020. From CO or CO₂? Space-resolved insights into high-pressure CO₂ hydrogenation to methanol over Cu/ZnO/Al₂O₃. *Catalysis Science* 10, 2763–2768. <https://doi.org/10.1039/D0CY00050G>.
- Gervasini, A., Bennici, S., 2005. Dispersion and surface states of copper catalysts by temperature-programmed-reduction of oxidized surfaces (s-TPR). *Appl. Catal. A* 281, 199–205. <https://doi.org/10.1016/j.apcata.2004.11.030>.
- Grabow, M.M., 2011. Mechanism of methanol synthesis on Cu through CO₂ and CO hydrogenation. *ACS Catal.* 1, 365–384. <https://doi.org/10.1021/cs200055d>.

- Graciani, J., Mudiyansele, K., Xu, F., Baber, A.E., Evans, J., Senanayake, S.D., Stacchiola, D.J., Liu, P., Hrbek, J., Sanz, J.F., 2014. Highly active copper-ceria and copper-ceria-titania catalysts for methanol synthesis from CO₂. *Science* 345, 546–550. <https://doi.org/10.1126/science.1253057>.
- Günter, M.M., Ressler, T., Bems, B., Büscher, C., Genger, T., Hinrichsen, O., Muhler, M., Schlögl, R., 2001. Implication of the microstructure of binary Cu/ZnO catalysts for their catalytic activity in methanol synthesis. *Catal. Lett.* 71, 37–44. <https://doi.org/10.1023/A:1016696022840>.
- Guo, X., Mao, D., Lu, G., Wang, S., Wu, G., 2011. The influence of La doping on the catalytic behavior of Cu/ZrO₂ for methanol synthesis from CO₂ hydrogenation. *J. Mol. Catal. A: Chem.* 345, 60–68. <https://doi.org/10.1016/j.molcata.2011.05.019>.
- Jansen, W., Beckers, J., vd Heuvel, J., vd Gon, A.D., Bliet, A., Brongersma, H., 2002. Dynamic behavior of the surface structure of Cu/ZnO/SiO₂ catalysts. *Journal of Catalysis* 210, 229–236. [10.1006/jcat.2002.3679](https://doi.org/10.1006/jcat.2002.3679)
- Jung, K.T., Bell, A.T., 2002. Effects of zirconia phase on the synthesis of methanol over zirconia-supported copper. *Catal. Lett.* 80, 63–68. <https://doi.org/10.1023/A:1015326726898>.
- Kattel, S., Yan, B., Yang, Y., Chen, J.G., Liu, P., 2016. Optimizing Binding Energies of Key Intermediates for CO₂ hydrogenation to Methanol over Oxide-Supported Copper. *J. American Chemical Society* 138, 12440–12450. <https://doi.org/10.1021/jacs.6b05791>.
- Kattel, S., Ramirez, P.J., Chen, J.G., Rodriguez, J.A., Liu, P., 2017. Active sites for CO₂ hydrogenation to methanol on Cu/ZnO catalysts. *Science* 355, 1296–1299. <https://doi.org/10.1126/science.aal3573>.
- Kondrat, S.A., Smith, P.J., Lu, L., Bartley, J.K., Taylor, S.H., Spencer, M.S., Kelly, G.J., Park, C.W., Kiely, C.J., Hutchings, G.J., 2018. Preparation of a highly active ternary Cu-Zn-Al oxide methanol synthesis catalyst by supercritical CO₂ antisolvent precipitation. *Catal. Today* 317, 12–20. <https://doi.org/10.1016/j.cattod.2018.03.046>.
- Kondrat, S.A., Smith, P.J., Wells, P.P., Chater, P.A., Carter, J.H., Morgan, D.J., Fioridaliso, E.M., Wagner, J.B., Davies, T.E., Lu, L., 2016. Stable amorphous georgite as a precursor to a high-activity catalyst. *Nature* 531, 83–87. <https://doi.org/10.1038/d.2015.0008102108>.
- Köppel, R.A., Stöcker, C., Baiker, A., 1998. Copper-and silver-zirconia aerogels: preparation, structural properties and catalytic behavior in methanol synthesis from carbon dioxide. *J. Catal.* 179, 515–527. <https://doi.org/10.1006/jcat.1998.2252>.
- Kühl, S., Tarasov, A., Zander, S., Kasatkin, I., Behrens, M., 2014. Cu-Based Catalyst Resulting from a Cu, Zn, Al Hydroxalite-Like Compound: A Microstructural, Thermoanalytical, and In Situ XAS Study. *Chemistry—A European J.* 20, 3782–3792. <https://doi.org/10.1002/chem.201302599>.
- Kuld, S., Conradsen, C., Moses, P.G., Chorkendorff, I., Sehested, J., 2014. Quantification of zinc atoms in a surface alloy on copper in an industrial-type methanol synthesis catalyst. *Angew. Chem.* 126, 6051–6055. <https://doi.org/10.1002/ange.201311073>.
- Lam, E., Lamier, K., Wolf, P., Tada, S., Safonova, O., Copéret, C., 2018. Isolated Zr Surface Sites on Silica Promotes Hydrogenation of CO₂-to-CH₃OH in Supported Cu Catalysts. *J. Am. Chem. Soc.* 140, 10530–10535. <https://doi.org/10.1021/jacs.8b05595>.
- Larmier, K., Liao, W.C., Tada, S., Lam, E., Verel, R., Bansode, A., Urakawa, A., Comas-Vives, A., Copéret, C., 2017. CO₂-to-methanol hydrogenation on zirconia-supported copper nanoparticles: reaction intermediates and the role of the metal-support interface. *Angew. Chem. Int. Ed.* 56, 2318–2323. <https://doi.org/10.1002/anie.201610166>.
- Li, M.M.-J., Zeng, Z., Liao, F., Hong, X., Tsang, S.C.E., 2016. Enhanced CO₂ hydrogenation to methanol over CuZn nanoalloy in Ga modified Cu/ZnO catalysts. *J. Catal.* 343, 157–167. <https://doi.org/10.1016/j.jcat.2016.03.020>.
- Li, K., Chen, J.G., 2019. CO₂ hydrogenation to methanol over ZrO₂-Containing Catalysts: Insights into ZrO₂ Induced Synergy. *ACS Catal.* 9, 7840–7861. <https://doi.org/10.1021/acscatal.9b01943>.
- Liang, B., Ma, J., Su, X., Yang, C., Duan, H., Zhou, H., Deng, S., Li, L., Huang, Y., 2019. Investigation on deactivation of Cu₂ZnO/Al₂O₃ catalyst for CO₂ hydrogenation to methanol. *Industrial Engineering Chemistry Research* 58, 9030–9037. <https://doi.org/10.1021/acs.iecr.9b01546>.
- Ma, Z.-Y., Yang, C., Wei, W., Li, W.-H., Sun, Y.-H., 2005. Catalytic performance of copper supported on zirconia polymorphs for CO hydrogenation. *J. Mol. Catal. A: Chem.* 231, 75–81. <https://doi.org/10.1016/j.molcata.2004.12.026>.
- Ma, Y., Wang, J., Goodman, K.R., Head, A.R., Tong, X., Stacchiola, D.J., White, M.G., 2020. Reactivity of a Zirconia-Copper Inverse Catalyst for CO₂ hydrogenation. *J. Physical Chemistry C* 124, 22158–22172. <https://doi.org/10.1021/acs.jpcc.0c06624>.
- Martin, O., Martín, A.J., Mondelli, C., Mitchell, S., Segawa, T.F., Hauer, R., Drouilly, C., Curulla-Ferré, D., Pérez-Ramírez, J., 2016. Indium oxide as a superior catalyst for methanol synthesis by CO₂ hydrogenation. *Angew. Chem. Int. Ed.* 55, 6261–6265. <https://doi.org/10.1002/anie.201600943>.
- Martinez-Suarez, L., Siemer, N., Frenzel, J., Marx, D., 2015. Reaction network of methanol synthesis over Cu/ZnO nanocatalysts. *ACS Catal.* 5, 4201–4218. <https://doi.org/10.1021/acscatal.5b00442>.
- Men, Y.-L., Liu, Y., Wang, Q., Luo, Z.H., Shao, S., Li, Y.-B., 2019. Highly dispersed Pt-based catalysts for selective CO₂ hydrogenation to methanol at atmospheric pressure. *Chem. Eng. Sci.* 200, 167–175. <https://doi.org/10.1016/j.ces.2019.02.004>.
- Nakamura, I., Fujitani, T., Uchijima, T., Nakamura, J., 1996. A model catalyst for methanol synthesis: Zn-deposited and Zn-free Cu surfaces. *J. Vacuum Science Technology A: Vacuum, Surfaces Films* 14, 1464–1468. <https://doi.org/10.1116/1.579970>.
- Reichenbach, T., Mondal, K., Jäger, M., Vent-Schmidt, T., Himmel, D., Dybbert, V., Bruix, A., Krossing, I., Walter, M., Moseler, M., 2018. Ab initio study of CO₂ hydrogenation mechanisms on inverse ZnO/Cu catalysts. *J. Catal.* 360, 168–174. <https://doi.org/10.1016/j.jcat.2018.01.035>.
- Rhodes, M.D., Bell, A.T., 2005. The effects of zirconia morphology on methanol synthesis from CO and H₂ over Cu/ZrO₂ catalysts: Part I Steady-state studies. *J. Catalysis* 233, 198–209. <https://doi.org/10.1016/j.jcat.2005.04.026>.
- Ro, I., Liu, Y., Ball, M.R., Jackson, D.H., Chada, J.P., Sener, C., Kuech, T.F., Madon, R.J., Huber, G.W., Dumesic, J.A., 2016. Role of the Cu-ZrO₂ interfacial sites for conversion of ethanol to ethyl acetate and synthesis of methanol from CO₂ and H₂. *ACS Catal.* 6, 7040–7050. <https://doi.org/10.1021/acscatal.6b01805>.
- Rungtaweeworanit, B., Baek, J., Araujo, J.R., Archanjo, B.S., Choi, K.M., Yaghi, O. M., Somorjai, G.A., 2016. Copper nanocrystals encapsulated in Zr-based metal-organic frameworks for highly selective CO₂ hydrogenation to methanol. *Nano Lett.* 16, 7645–7649. <https://doi.org/10.1021/acs.nanolett.6b03637>.
- Sadeghinia, M., Rezaei, M., Kharat, A.N., Jorabchi, M.N., Nematollahi, B., Zareiekordshouli, F., 2020. Effect of In₂O₃ on the structural properties and catalytic performance of the CuO/ZnO/Al₂O₃ catalyst in CO₂ and CO hydrogenation to methanol. *Molecular Catalysis* 484. <https://doi.org/10.1016/j.mcat.2020.110776>.
- Samson, K., Sliwa, M., Socha, R.P., Góra-Marek, K., Mucha, D., Rutkowska-Zbik, D., Paul, J., Ruggiero-Mikołajczyk, M., Grabowski, R., Słoczyński, J., 2014. Influence of ZrO₂ structure and copper electronic state on activity of Cu/ZrO₂ catalysts in methanol synthesis from CO₂. *ACS Catal.* 4, 3730–3741. <https://doi.org/10.1021/cs500979c>.
- Senanayake, S.D., Ramirez, P.J., Waluyo, I., Kundu, S., Mudiyansele, K., Liu, Z., Liu, Z., Ananda, S., Stacchiola, D.J., Evans, J., 2016. Hydrogenation of CO₂ to Methanol on CeO_x/Cu(111) and ZnO/Cu(111) Catalysts: Role of the Metal-Oxide Interface and Importance of Ce³⁺ Sites. *J. Physical Chemistry C* 120, 1778–1784. <https://doi.org/10.1021/acs.jpcc.5b12012>.
- Shi, Z., Tan, Q., Tian, C., Pan, Y., Sun, X., Zhang, J., Wu, D., 2019. CO₂ hydrogenation to methanol over Cu-In intermetallic catalysts: Effect of reduction temperature. *J. Catal.* 379, 78–89. <https://doi.org/10.1016/j.jcat.2019.09.024>.
- Słoczyński, J., Grabowski, R., Olszewski, P., Kozłowska, A., Stoch, J., Lachowska, M., Skrzypek, J., 2006. Effect of metal oxide additives on the activity and stability of Cu/ZnO/ZrO₂ catalysts in the synthesis of methanol from CO₂ and H₂. *Appl. Catal. A* 310, 127–137. <https://doi.org/10.1016/j.apcata.2006.05.035>.
- Studt, F., Behrens, M., Kunkes, E.L., Thomas, N., Zander, S., Tarasov, A., Schumann, J., Frei, E., Varley, J.B., Abild-Pedersen, F., 2015. The mechanism of CO and CO₂ hydrogenation to methanol over Cu-based catalysts. *ChemCatChem* 7, 1105–1111. <https://doi.org/10.1002/cctc.201500123>.
- Tada, S., Katagiri, A., Kiyota, K., Honma, T., Kamei, H., Nariyuki, A., Uchida, S., Satokawa, S., 2018a. Cu species incorporated into amorphous ZrO₂ with high activity and selectivity in CO₂-to-methanol hydrogenation. *J. Physical Chemistry C* 122, 5430–5442. <https://doi.org/10.1021/acs.jpcc.7b11284>.
- Tada, S., Kayamori, S., Honma, T., Kamei, H., Nariyuki, A., Kon, K., Toyao, T., Shimizu, K.-I., Satokawa, S., 2018b. Design of interfacial sites between Cu and amorphous ZrO₂ dedicated to CO₂-to-methanol hydrogenation. *ACS Catal.* 8, 7809–7819. <https://doi.org/10.1021/acscatal.8b01396>.
- Tarasov, A., Schumann, J., Girgsdies, F., Thomas, N., Behrens, M., 2014. Thermokinetic investigation of binary Cu/Zn hydroxycarbonates as precursors for Cu/ZnO catalysts. *Thermochim Acta* 591, 1–9. <https://doi.org/10.1016/j.tca.2014.04.025>.
- Topsøe, H., Ovesen, C., Clausen, B., Topsøe, N.-Y., Nielsen, P.H., Törnqvist, E., Nørskov, J., 1997. Importance of dynamics in real catalyst systems. *Studies in Surface Science and Catalysis*. Elsevier, 121–139. [https://doi.org/10.1016/S0167-2991\(97\)80402-8](https://doi.org/10.1016/S0167-2991(97)80402-8).
- Topsøe, N.-Y., Topsøe, H., 1999. FTIR studies of dynamic surface structural changes in Cu-based methanol synthesis catalysts. *J. Mol. Catal. A: Chem.* 141, 95–105. [https://doi.org/10.1016/S1381-1169\(98\)00253-2](https://doi.org/10.1016/S1381-1169(98)00253-2).
- Van Den Berg, R., Prieto, G., Korpershoek, G., Van Der Wal, L.I., Van Bunningen, A.J., Lægsgaard-Jørgensen, S., De Jongh, P.E., De Jong, K.P., 2016. Structure sensitivity of Cu and CuZn catalysts relevant to industrial methanol synthesis. *Nat. Commun.* 7, 1–7. <https://doi.org/10.1038/ncomms13057>.
- Van Der Grift, C., Wielers, A., Jogh, B., Van Beunum, J., De Boer, M., Versluijs-Helder, M., Geus, J., 1991. Effect of the reduction treatment on the structure and reactivity of silica-supported copper particles. *J. Catal.* 131, 178–189. [https://doi.org/10.1016/0021-9517\(91\)90334-Z](https://doi.org/10.1016/0021-9517(91)90334-Z).
- Wang, G., Mao, D., Guo, X., Yu, J., 2019a. Methanol synthesis from CO₂ hydrogenation over CuO-ZnO-ZrO₂-M₂O₃ catalysts (M = Cr, Mo and W). *Int. J. Hydrogen Energy* 44, 4197–4207. <https://doi.org/10.1016/j.ijhydene.2018.12.131>.
- Wang, Y., Kattel, S., Gao, W., Li, K., Liu, P., Chen, J.G., Wang, H., 2019b. Exploring the ternary interactions in Cu-ZnO-ZrO₂ catalysts for efficient CO₂ hydrogenation to methanol. *Nat. Commun.* 10, 1–10. <https://doi.org/10.1038/s41467-019-09072-6>.
- Witoon, T., Chalorngtham, J., Dumrongbunditkul, P., Chareonpanich, M., Limtrakul, J., 2016. CO₂ hydrogenation to methanol over Cu/ZrO₂ catalysts: Effects of zirconia phases. *Chem. Eng. J.* 293, 327–336. <https://doi.org/10.1016/j.cej.2016.02.069>.
- Wu, C., Lin, L., Liu, J., Zhang, J., Zhang, F., Zhou, T., Rui, N., Yao, S., Deng, Y., Yang, F., Xu, W., Luo, J., 2020. Inverse ZrO₂/Cu as a highly efficient methanol synthesis catalyst from CO₂ hydrogenation. *Nat. Commun.* 11, 5767. <https://doi.org/10.1038/s41467-020-19634-8>.

- Zabilskiy, M., Sushkevich, V.L., Palagin, D., Newton, M.A., Krumeich, F., van Bokhoven, J.A., 2020. The unique interplay between copper and zinc during catalytic carbon dioxide hydrogenation to methanol. *Nat. Commun.* 11, 1–8. <https://doi.org/10.1038/s41467-020-16342-1>.
- Zhang, G., Fan, G., Yang, L., Li, F., 2020. Tuning surface-interface structures of ZrO₂ supported copper catalysts by in situ introduction of indium to promote CO₂ hydrogenation to methanol. *Appl. Catal. A* 117805. <https://doi.org/10.1016/j.apcata.2020.117805>.
- Zhao, Y., Shan, B., Wang, Y., Zhou, J., Wang, S., Ma, X., 2018. An effective CuZn–SiO₂ bimetallic catalyst prepared by hydrolysis precipitation method for the hydrogenation of methyl acetate to ethanol. *Industrial Engineering Chemistry Research* 57, 4526–4534. <https://doi.org/10.1021/acs.iecr.7b05391>.
- Zheng, H., Narkhede, N., Han, L., Zhang, H., Li, Z., 2020. Methanol synthesis from CO₂: a DFT investigation on Zn-promoted Cu catalyst. *Res. Chem. Intermed.* 46, 1749–1769. <https://doi.org/10.1007/s11164-019-04061-2>.